A molecular dynamics study of sub- and supercritical water using a polarizable potential model

ARTICLE *in* THE JOURNAL OF CHEMICAL PHYSICS · SEPTEMBER 1998

Impact Factor: 2.95 · DOI: 10.1063/1.477098

4 AUTHORS, INCLUDING:

Noriyuki Yoshii
Nagoya University
34 PUBLICATIONS **379** CITATIONS

SEE PROFILE

A molecular dynamics study of sub- and supercritical water using a polarizable potential model

Noriyuki Yoshii, Hiromi Yoshie, Shinichi Miura, and Susumu Okazaki[a)]
Department of Electronic Chemistry, Tokyo Institute of Technology, 4259 Nagatsuta, Midori-ku, Yokohama 226-8502, Japan

(Received 28 May 1998; accepted 19 June 1998)

A series of molecular dynamics calculations for water has been carried out along an isochore at 1 g/cm^3 and an isotherm at 600 K in order to examine microscopic properties of water in the sub- and supercritical states. A polarizable potential model proposed by Dang (RPOL model) was employed to take into account the state dependence of intermolecular interaction. Along the isochore, fluid structure changes from tetrahedral icelike structure at room temperature to simple-liquidlike one at high temperatures. Orientational correlation between a tagged molecule and its neighbors is reduced substantially with increasing temperature, though hydrogen bonds between two molecules persist even at 600 K. As temperature increases, the number of the hydrogen bonds per molecule decreases monotonically from 3.2 at 280 K to 1.9 at 600 K. The activation barrier for diffusion at 600 K is about half as large as that at room temperature. A collective polarization relaxation loses collective character above the temperature where the structural change occurs. Along the isotherm, on the other hand, the long-ranged tail of radial distribution functions was observed near the critical density ρ_c. Ornstein-Zernike behavior, however, was not found owing to the present small system. The number of hydrogen bonds decreases almost linearly as a function of the density from 1.9 at 1 g/cm^3 to 0 in the gas limit. However, the hydrogen bonds were still found near the critical density. At densities below ρ_c, density dependence of the diffusion coefficients are qualitatively described by the simple kinetic theory for gases. At higher densities, the diffusion coefficients deviate from the prediction by the kinetic theory. Rotational correlation function at low density has the form similar to free rotors, while at high densities, the rotational relaxation may be described by rotational diffusion. It indicates that the rotational dynamics changes continuously around the critical density from a gaslike one to a liquidlike one. © *1998 American Institute of Physics.* [S0021-9606(98)01436-6]

I. INTRODUCTION

Recently, water in a supercritical (SC) state has attracted remarkable interest in the field of chemical engineering.[1–8] In the SC state, for example, density of the system can be easily controlled from a liquidlike one to a gaslike one by reducing pressure. Thus, various properties of the fluid, for example solubility of molecules, change continuously, which enables us to produce fine particles and thin films by relatively simple processes. The SC water is also employed as an efficient solvent for the hydrolysis of hazardous chemicals. In this case, the SC water plays a role not only as an effective medium of the reaction but also as an acid catalyst in itself. From a microscopic viewpoint, solvation of molecules and chemical reactions including water molecules play an essential role in describing the above chemical processes. In order to understand the chemical processes in the SC water, molecular based characterization of the fluid such as local density fluctuation and, in particular, hydrogen bonding between molecules, needs to be done first. The purpose of the present study is to make clear the microscopic structure and dynamics of water at the extreme condition based upon molecular dynamics (MD) calculations.

Fluid structure of water has been characterized by atomic pair correlation functions: oxygen-oxygen, oxygen-hydrogen, and hydrogen-hydrogen pair correlation functions. At ambient condition, the first peak of oxygen-hydrogen radial distribution function (RDF) around 1.8 Å is a manifestation of hydrogen bonding between molecules. Computer calculations with common empirical potential models have successfully reproduced this hydrogen-bonding peak for the ambient water.[9,10] To investigate the properties of the hydrogen bonds at extreme condition, the calculation studies have been extended to the supercritical state.[11–22] The molecular dynamics calculation with the TIP4P model indicated that 70% of the hydrogen bonds existing in the ambient water still remain at temperatures up to 1130 K.[11] The first experimental study of the fluid structure for the SC water has been performed by Postorino *et al.*[23] They obtained the oxygen-oxygen, oxygen-hydrogen, and hydrogen-hydrogen RDFs by neutron diffraction experiment using the isotopic substitution technique. They found that the first peak of oxygen-hydrogen RDF completely disappeared in the supercritical state at 400 °C and 0.66 g/cm^3. It suggests that the hydrogen bonds between molecules do not exist at the supercritical condition in spite of the fact that the hydrogen-bonding energy is well above thermal energy at 400 °C. The discrepancy between

a)Author to whom correspondence should be addressed.

the calculations and the experiment gave rise to much controversy about the persistence of the hydrogen bonds in the supercritical state. Postorino *et al.* suggested that the reason for this discrepancy is due to the deficiency of the pairwise additive potential model such as TIP4P models. On the other hand, however, Löffler *et al.*[13] claimed that the discrepancy arises from the inelasticity correction to the neutron data, which is particularly large for the light water sample. They showed that the form of RDFs is very sensitive to the inelasticity correction. According to Löffler and his co-workers' suggestion. Soper *et al.*[24] reexamined the neutron diffraction data using a new method to obtain more reliable pair correlation functions. The revised analysis was in better agreement with the calculation results. An X-ray diffractometry[25] and a recent nuclear magnetic resonance experiment[26] also showed that the hydrogen bonds between water molecules persist even in the supercritical state. However, the picture of hydrogen bonding in the supercritical water is still different between the calculations and the experiments.

The most important point, here, in describing intermolecular interactions is electrostatic interactions. Among the above calculation studies, fixed point charge models were employed.[11,12,14–16] Typical examples are SPC and TIP4P models. These potential parameters are optimized to reproduce the properties of liquid water at the ambient condition at 298 K and 1 g/cm^3. However, we must be careful in the fact that the dipole moment of an isolated water molecule is 1.85 D.[27] In condensed phases, however, charge distribution in the molecule is reorganized by the electrostatic field from the other molecules. The experimental value of the dipole moment in ice becomes 2.6 D.[28] In the fluid phase, the dipole moment must have intermediate values between those in the gas and the ice. Clearly, thus, it is not sufficient to describe the properties of water over a wide range of physical states based upon this kind of fixed-charge potential model. Now, the model should include the polarization effect of the molecule to describe the intermolecular interaction in the sub- and supercritical states. Car-Parrinello *ab initio* MD is one of the best methodologies to take into account the state dependence of intermolecular interactions. Fois *et al.*[17] carried out the *ab initio* MD calculation of the SC water. They calculated the static structure factors and discussed the short-ranged structure of the SC water. The method is, however, computationally expensive. In this sense, we need simpler models to investigate the properties of water over a wide range of thermodynamic states. A natural improvement of the empirical potential model is to introduce polarizabilities to water molecules. In this model, the molecular induced dipole moments are determined self-consistently with electrostatic field reflecting the configuration of the fluid which depends on the physical state. Thus, we employed a polarization model of water, the RPOL model,[29] in order to take account of the state-dependent interaction. As reported in our previous paper, critical constants for the RPOL model fluid are $T_c = 561$ K, $\rho_c = 0.30$ g/cm^3, and $P_c = 331$ bar.[30]

While interest in the previously reported studies has been mainly focused on the persistence of the hydrogen bond in the SC water,[11–14,17–22,26] connection between the structure and dynamics of sub- and supercritical water has not yet been well established. In this study, we examined systematically the microscopic structure and dynamics of the sub- and supercritical water using the RPOL model over a wide range of state points. The temperature-dependent and density-dependent properties were separately investigated based on the MD calculations along an isochore at 1 g/cm^3 ($=3.4\rho_c$) and an isotherm at 600 K ($=1.07T_c$). In particular, we paid special attention to the effect of structural change of the fluid on both translational and rotational motion of the water molecules.

TABLE I. The potential parameters of the RPOL model.

	ϵ/K	σ/Å	Q/esu	α/Å^3
O	80.75	3.196	−0.730	0.53
H	0.0	0.0	−0.365	0.18

The paper is organized as follows. Computational details are described in Sec. II. In Sec. III, distribution of molecular polarization is presented for various physical states. Structural and dynamic properties of sub- and supercritical water along an isochore at 1 g/cm^3 and along an isotherm at 600 K, respectively, are discussed in detail in Secs. IV and V, respectively. The conclusion is presented in Sec. VI.

II. COMPUTATIONAL DETAILS

A. Polarizable potential model

In this study, we employed a polarizable potential model of a water molecule, which includes atomic polarization on each atomic site. Then, the intermolecular interaction depends on electrostatic field by the surrounding molecules. We used the polarizable potential model developed by Dang,[29] the RPOL model. The molecular geometry is the same as the SPC model, oxygen-hydrogen bond length $R_{\mathrm{OH}} = 1$ Å and bond angle $\angle \mathrm{HOH} = 109.5°$. Each atomic site i has a fixed charge Q_i and isotropic polarizability α_i. A permanent dipole moment composed of the point charges in a molecule is 2.02 D. Lennard-Jones (LJ) interaction between molecules is given by oxygen-oxygen separation with diameter σ and well depth ϵ. Potential parameters for the RPOL model are listed in Table I. Total potential energy of the system is given by the sum of LJ interaction, charge-charge interaction, induced dipole-charge interaction, induced dipole-induced dipole interaction, and self-energy. An explicit expression of the potential energy is, thus, presented by

$$V = \frac{1}{2}\sum_{i}^{N}\sum_{j\neq i}^{N} 4\epsilon\left[\left(\frac{\sigma}{r_{ij}}\right)^{12} - \left(\frac{\sigma}{r_{ij}}\right)^{6}\right] + \frac{1}{2}\sum_{i}^{3N}\sum_{j\neq i}^{3N}\frac{Q_i Q_j}{r_{ij}} - \sum_{i}^{3N}\mathbf{p}_i^I\cdot\mathbf{E}_i^0 - \frac{1}{2}\sum_{i}^{3N}\sum_{j\neq i}^{3N}\mathbf{p}_i^I\cdot\mathbf{T}_{ij}\cdot\mathbf{p}_j^I + \sum_{i}^{3N}\frac{\mathbf{p}_i^I\cdot\mathbf{p}_i^I}{2\alpha_i}, \tag{1}$$

where N is the number of water molecules, $\mathbf{p}_i^I$ and $\mathbf{E}_i^0$ are the

induced dipole moment and the electrostatic field by point charges of other molecules, respectively. The dipole moment tensor $\mathbf{T}_{ij}$ is

$$\mathbf{T}_{ij}=\frac{3}{r^5}\begin{pmatrix} x^2 & xy & xz \\ xy & y^2 & yz \\ xz & yz & z^2 \end{pmatrix}-\frac{1}{r^3}\begin{pmatrix} 1 & 0 & 0 \\ 0 & 1 & 0 \\ 0 & 0 & 1 \end{pmatrix}. \tag{2}$$

Induced dipole moment on an atomic site i, $\mathbf{p}_i^I$, is obtained by the following equation:

$$\mathbf{p}_i^I=\alpha_i\mathbf{E}_i=\alpha_i\left(\mathbf{E}_i^0+\sum_{j\neq i}^{3N}\mathbf{T}_{ij}\cdot\mathbf{p}_j^I\right), \quad i=1,\ldots,3N. \tag{3}$$

We solved Eq. (3) iteratively at each MD step. The iterative calculation was terminated when the following self-consistency condition was satisfied:

$$\sqrt{\frac{\Sigma_i^{3N}|\mathbf{p}_i^{I,k+1}-\mathbf{p}_i^{I,k}|^2}{3N}}\leqslant 3\times 10^{-5}\mathrm{D}. \tag{4}$$

Typically, five or six iterations were needed at each MD step. This condition gives the error per molecule

$$\Delta\mathbf{p}_i^I\equiv\frac{|\mathbf{p}_i^{I,k+1}|-|\mathbf{p}_i^{I,k}|}{|\mathbf{p}_i^{I,k+1}|}\approx 0.02. \tag{5}$$

The threshold of iterative calculation was determined in such a way that the Hamiltonian of the system was conserved, the error being less than 10^{-4} of the total energy over 10 ps. The calculated potential energy and average molecular dipole moment were in good agreement with the values reported by Dang.[29]

B. Calculation method

Molecular dynamics calculations have been performed in canonical ensemble using Nosé thermostat.[31] The cubic basic cell contained 256 water molecules in the periodic boundary condition. The potential cutoff distance was half of the cell length. Long range LJ interaction beyond the cutoff distance was corrected for the virial and potential energy. All the electrostatic interactions including induced dipole-charge and induced dipole-induced dipole interactions were calculated by means of Ewald summation technique. Equation of motion was integrated by the Gear's predictor corrector method with a time step of $\Delta t=0.5$ fs.[32] In Fig. 1, state points investigated in this study are presented together with the critical point and liquid-vapor coexistence line for the RPOL model reported previously.[30] 60 000~400 000 steps (30~200 ps) of the calculation were needed for each state point to reach satisfactory statistical accuracy.

C. Definition of hydrogen bond

Here, we define the hydrogen bond between water molecules. We regard two molecules as hydrogen bonded when the following two conditions are satisfied simultaneously: (1) oxygen-hydrogen separation is closer than a threshold distance r_{OH}, and (2) interaction energy between two molecules is lower than a threshold value E_{HB}. The former threshold is called geometry criterion and the latter energy criterion.

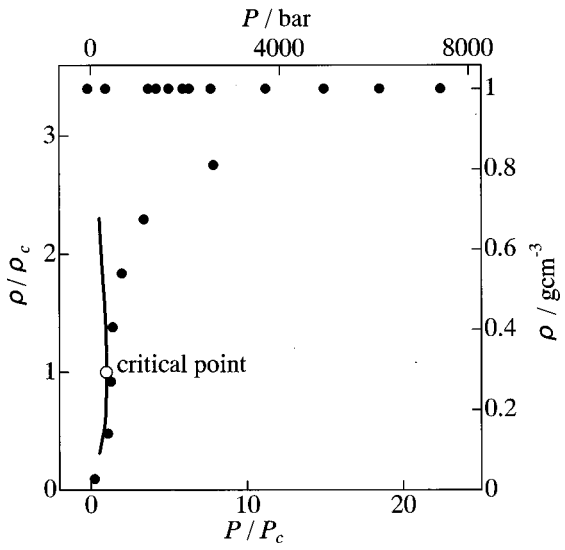

FIG. 1. Calculated state points reduced by critical density and critical pressure. Open circle represents the critical point and solid line the liquid-vapor coexistence curve. Closed circles are the state points along an isochore at 1 g/cm^3 and along an isotherm at 600 K, where MD calculations have been performed.

Only one of these two criteria has usually been adopted to define the hydrogen bond at ambient condition. Kalinichev and Bass,[14] however, showed that only with the geometry criterion, too many molecules were detected as hydrogen-bonded under high pressure conditions. At 10 GPa, for example, 8% of molecules in the system had eight hydrogen bonds. Since the number of unstable molecules increases in the first coordination shell at the extreme conditions, a combination of energy and geometry criteria gives a better definition for the hydrogen bond. The energetically unstable molecules are then removed. In this study, we used 2.5 Å as r_{OH}, which corresponds to the position of the first minimum of the oxygen-hydrogen radial distribution function. It is a convenient definition since the position of the minimum is almost independent of the temperature and density. This will be shown later. In order to determine the threshold of the energy criteria, we examined state dependence of the pair interaction energy. The distribution functions of the pair interaction energy for three selected state points are shown in Fig. 2. At ambient condition, there exists a peak around -27 kJ/mol, representing a moderately stable pair of molecules. This may be assigned to the hydrogen bonding in the liquid. At the extreme conditions, the hydrogen bond peak diminishes and the population of higher energy pairs increases. To extract the moderately stable pairs of molecules, we used the energy criteria of -14 kJ/mol corresponding to the position of the minimum in the pair energy distribution function at the ambient condition.

III. DISTRIBUTION OF MOLECULAR POLARIZATION

In this section, we show the state dependence of the molecular polarization. The isolated RPOL water has the dipole moment of 2.02 D, which comes from fixed charges in the model. In the fluid phase, electrostatic field from the

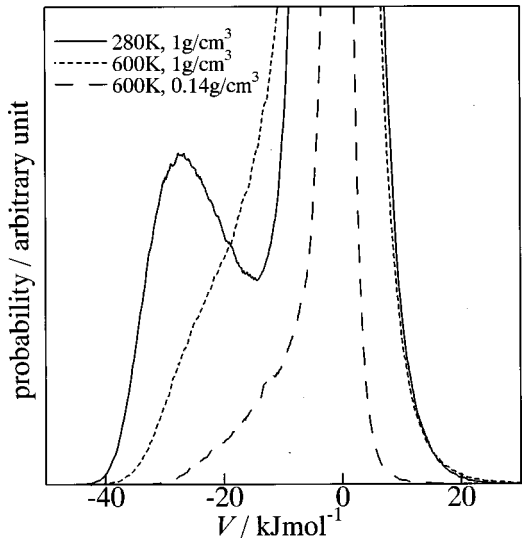

FIG. 2. Distribution of pair potential energy.

medium induces the additional dipole moment on the molecule. The molecular dipole moment, then, may be described by sum of the above two components,

$$\mathbf{p}_i = \mathbf{p}_i^0 + \mathbf{p}_i^I, \tag{6}$$

where $\mathbf{p}_i^0$ and $\mathbf{p}_i^I$ denote the permanent and induced dipole moment of molecule i, respectively. In Fig. 3, we show the distribution function of the absolute value of the dipole moment of water in various physical states. The figure clearly shows an importance of the induced dipole moment when we describe the interaction depending on the physical states. At 280 K and 1 g/cm^3, the averaged molecular dipole moment has the value of 2.54 D where approximately symmetric distribution is found. As temperature increases along an isochore at 1 g/cm^3, $\langle|\mathbf{p}_i|\rangle$ decreases monotonically and its distribution becomes broader. At 600 K, $\langle|\mathbf{p}_i|\rangle$ becomes 2.39 D. On the other hand, as density decreases along an isotherm at 600 K, $\langle|\mathbf{p}_i|\rangle$ decreases monotonically again, and, its distribution becomes narrower. The asymmetry of the distribution, the tail in the larger dipole moment, arises with decreasing density. It suggests that even at the low density there persist the strongly interacting pairs of molecules, which must correspond to the hydrogen bonds. The detailed analyses at the molecular level will be presented in the following sections.

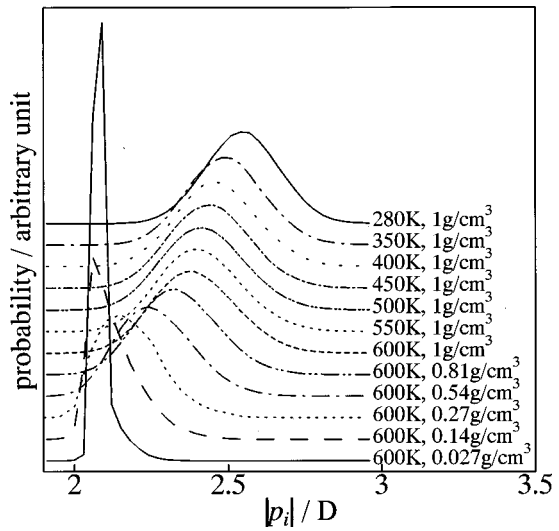

FIG. 3. Temperature and density dependence of distribution of single molecular dipole moment.

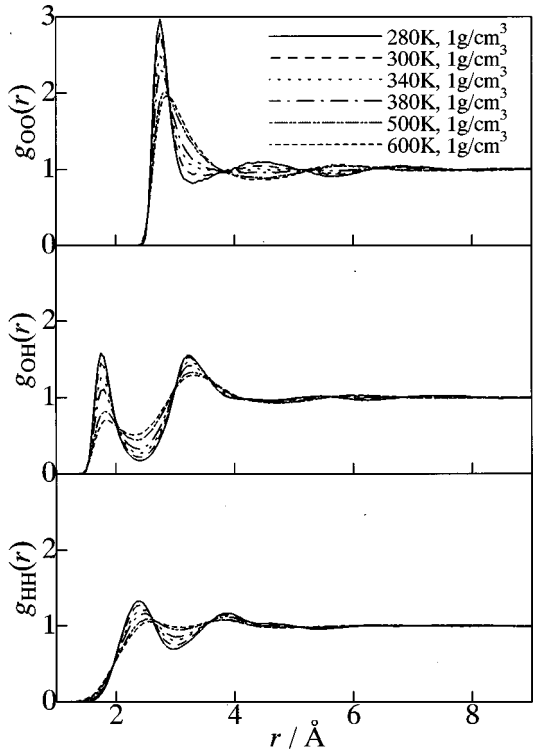

FIG. 4. Temperature dependence of oxygen-oxygen, oxygen-hydrogen, and hydrogen-hydrogen radial distribution functions, g_{OO}, g_{OH}, and g_{HH}, respectively, along an isochore at 1 g/cm^3. The results are plotted for the fluid at six state points.

IV. ISOCHORE AT 1 G/CM^3

In this section, we present temperature dependence of the static and dynamic properties of sub- and supercritical water based upon molecular trajectories along the isochore at 1 g/cm^3. Analyses have been carried out for 12 selected physical states between 280 and 600 K.

A. Spatial density correlation

Figure 4 shows the temperature dependence of oxygen-oxygen, oxygen-hydrogen, and hydrogen-hydrogen radial distribution functions, g_{OO}, g_{OH}, and g_{HH}, respectively. With regard to g_{OO}, both the first and second peaks shift to the larger separation with increasing temperature. At 280 K, the second peak is located at 4.5 Å, which is ascribed to the local tetrahedral icelike structure of water. This peak, thus, indicates implicitly the three body correlation of oxygen atoms.[33] As temperature increases, the second peak gradually moves outward and disappears around 360 K. This indicates that the three body correlation of oxygen atoms vanishes at the temperature. When the temperature increases further, the second peak appears again around 6.0 Å.[24,25,34] The behavior suggests a local fluid structure changes in this temperature

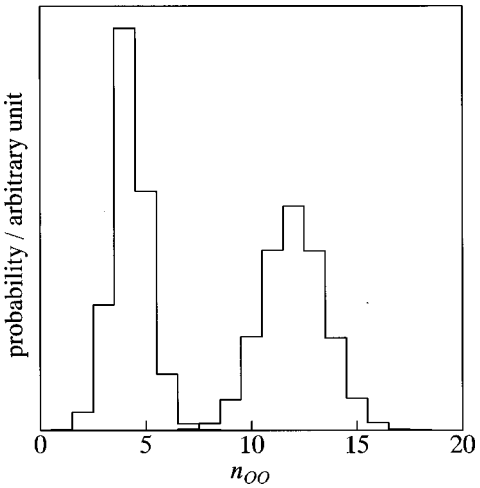

FIG. 5. Histogram of number of oxygen atoms in the first coordination shell. The radius of the shell is 3.3 Å for water at 280 K and 1 g/cm^3 (left) and 4.5 Å at 600 K and 1 g/cm^3 (right), which correspond to the first minimum of the g_{OO}.

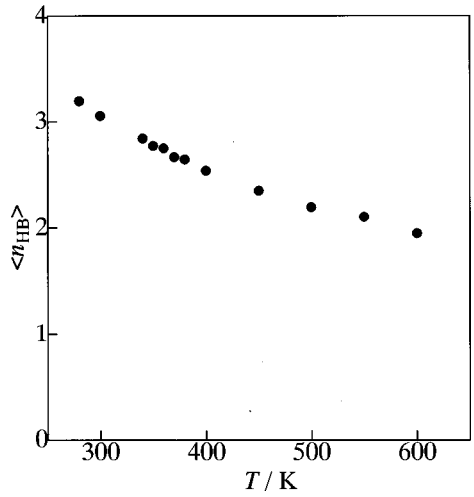

FIG. 6. Temperature dependence of average number of hydrogen bonds per molecule along an isochore at 1 g/cm^3. For definition, see the text.

range. The ratio of the second peak position to the first one gives a measure of local structure in the fluid. At 280 K, the ratio is 1.6, which is ascribed to the local tetrahedral coordination of water molecules as mentioned above. On the other hand, at 600 K, the ratio is 2.0, which is equivalent to that of simple liquids such as argon. This implies that fluid structure of oxygen (or center-of-mass of water molecule) at high temperatures is the same as simple liquids. We show the histogram of number of oxygen atoms found within the first coordination shell. The histogram was evaluated for the number of oxygen atoms in the coordination shell of a tagged oxygen. We adopted 3.3 Å as a definition of radius of the coordination shell at 280 K and 4.5 Å at 600 K, which correspond to the positions of the first minimum of g_{OO} at these temperatures. The results are shown in Fig. 5. At 280 K, the distribution shows the average coordination number of 4.2, corresponding to the tetrahedral coordination. At 600 K, the distribution becomes broader and the average coordination number is 12, which is again equivalent to that of the simple liquids. At the high temperatures, thus, center-of-mass of water has a simple-liquidlike structure.

From the viewpoint of the packing of molecules, the simple-liquidlike structure is preferable since the tetrahedral coordination needs larger intermolecular space. At room temperature, however, since the hydrogen-bonding energy well compensates the geometrical disadvantage, the tetrahedral local structure is formed.[33] As temperature increases, the tetrahedral local structure collapses due to the thermal fluctuation that makes the hydrogen bonding between molecules weaker. This was manifested by the disappearance of the second peak around 4.5 Å. Thus, at high temperatures, the local structure becomes the simple-liquidlike one. Here, it is worthwhile to consider a possibility of the phase transition for the change in g_{OO}. Our tentative conclusion, however, is that these two are in the same thermodynamic phase which may not be described by phase transition. This is demonstrated in the Appendix.

Concerning g_{OH}, the first and second peaks are located at the same positions at all temperatures investigated. As temperature increases, however, the first minimum at 2.5 Å becomes shallow and the first and second peaks become lower. It indicates that the larger thermal fluctuation makes the hydrogen bond weaker. The hydrogen bonds between water molecules, however, persist at 600 K, although the three body correlation of oxygen atoms is not found. With respect to g_{HH}, higher temperature makes the separation of the first and second peaks shorter, and the first minimum at 3 Å shallower. These features indicate that the orientational correlation between molecules becomes small with increasing temperature, which will be shown in detail in the next subsection. Further, it is noted that we can clearly see isosbestic points in all the radial distribution functions.[35] In general, the function, $g_{\mathrm{mix}}(r)=a\cdot g'(r)+b\cdot g''(r)$, has isosbestic points, where $g'(r)$ and $g''(r)$ are arbitrary functions and a and b are the arbitrary weights of the functions with a relation that $a+b=$constant. It might suggest the presence of two kinds of inherent liquid structures. However, it will need further investigations.

B. Hydrogen bond

Figure 6 shows temperature dependence of the average number of hydrogen bonds per molecule $\langle n_{HB} \rangle$, which corresponds to the average number of hydrogen-bonding molecules in the first coordination shell. At 280 K, $\langle n_{HB} \rangle$ is 3.2. This is in good agreement with the value reported by Kalinichev and Bass.[14] At the condition, the coordination number in the first shell is 4.2. Hence, 76% of molecules in the first coordination shell are hydrogen-bonded to the tagged molecule. As temperature increases, $\langle n_{HB} \rangle$ decreases and the coordination number increases monotonically. At 600 K, the average number of hydrogen bonds is 1.9, corresponding to 16% of the coordinated molecules. The behavior suggests that the orientational correlation almost diminishes between the tagged molecule and the coordinated water molecules.

Prior to seeing the orientational correlation, we characterize the hydrogen bond in the fluids. An isolated hydrogen-bonding pair of molecules can have a stable structure called

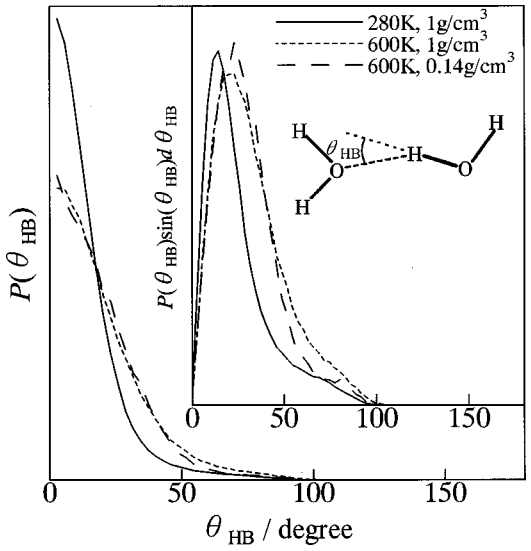

FIG. 7. Density distribution function of the angle θ_{HB} between O-H and H···O formed by a pair of hydrogen-bonding molecules in the first coordination shell. Actual number distribution function in the laboratory space is also presented in the inset.

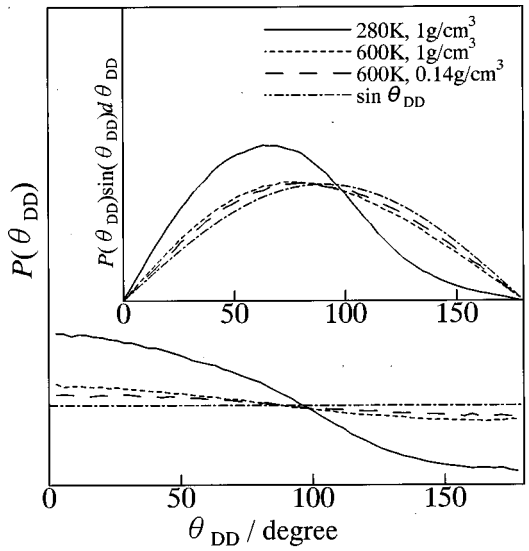

FIG. 8. Density distribution function of the angle θ_{DD} between the permanent dipole moments of the tagged molecule and the molecule in the first coordination shell. Actual number distribution function in the laboratory space is also presented in the inset.

a linear dimer. The linear dimer is characterized by the hydrogen bond formed by three atoms on a line, O-H···O. In the fluid, the hydrogen bond deviates from the ideal linear dimer. We first show the density distribution function of the angle between O-H and H···O, $P(\theta_{HB})$, in Fig. 7 for a few states of water. The distribution function was calculated for the hydrogen-bonded molecules. All the density distributions have a peak at 0°. Actual number distribution $P(\theta_{HB})\sin\theta_{HB}d\theta_{HB}$ in the laboratory space is also presented in the figure.[36] At 280 K, the number distribution has a peak at 14°, which indicates that the most probable hydrogen bond at the condition deviates from the ideal linear dimer by 14°. As temperature increases, the bending angle becomes large due to thermal fluctuation. The hydrogen bonds persisting at 600 K have the bending angle 21°, which gives weak orientational correlation.

In Fig. 8, we show both the density and the actual number distribution of the orientational correlation between two nearest neighbor molecules. The distribution function is plotted as a function of the angle θ_{DD} between the permanent dipole moments of the tagged molecule and the molecule in the first coordination shell. If there exists no orientational correlation between the two molecules, the density distribution is constant over θ_{DD} and the actual number distribution function is $\sin\theta_{DD}$. At room temperature, the density distribution function deviates markedly from the constant value, which indicates the existence of strong orientational correlation between the molecules. The number distribution functions have a peak at 65°, arising from the bended hydrogen bonds. In fact, the isolated linear dimer has the angle of 79° between the permanent dipole moments. As shown previously in Fig. 7, the bending angle with respect to the linear bond was 14°. The difference between these two angles gives the peak at 65°. At 600 K, both distribution functions approach the functions with no correlation. This indicates that the orientational correlation between molecules has almost disappeared at this temperature. The remaining small correlation comes from the hydrogen bonds persisting even at 600 K.

Next, we discuss the percolation of the hydrogen bonds in water using the average number of hydrogen bonds, $\langle n_{HB}\rangle$. Empirical observation has shown that the average number of bonds at percolation transition is about 1.5 for any lattice system.[37] If the average number of bonds is greater than the critical value, the system may be considered to be totally percolated by the bonds. For the ambient water, $\langle n_{HB}\rangle$ is 3.2. This is much greater than the percolation threshold. The ambient water may, thus, be regarded as percolated by the hydrogen bonds. In fact, it has been shown by many authors that water at ambient condition is filled up with percolated hydrogen bonds.[38] Now, it is interesting to find that even at 600 K, $\langle n_{HB}\rangle = 1.9$, which is still greater than the critical value. It suggests that, at least, according to the present definition for the hydrogen bond, the system is still percolated by the hydrogen bonds in spite of the disappearance of the second peak of g_{OO} around 4.5 Å.

C. Translational dynamics

Temperature dependence of the velocity autocorrelation function (VAF) of the oxygen atom is presented in Fig. 9. Since the oxygen atom is located at the position very close to the center of mass of the water molecule, we may regard the dynamics of the oxygen atom as that of the center of mass. At room temperature, there exists a damped oscillation in the VAFs. The oscillation has a period about 0.1 ps and damps after a few periods of the oscillation. This must come from the oscillation of molecules in a cage formed by surrounding molecules. As temperature increases, the oscillatory behavior becomes small and disappears at 600 K. The high temperature VAF has a functional form similar to that of simple dense liquids at high temperatures. This is the dynamical

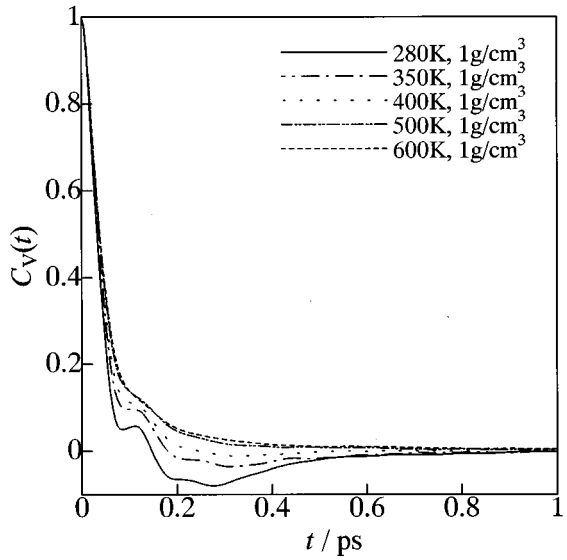

FIG. 9. Temperature dependence of velocity autocorrelation function of oxygen atom along an isochore at 1 g/cm^3. The result is plotted for the fluid at five state points.

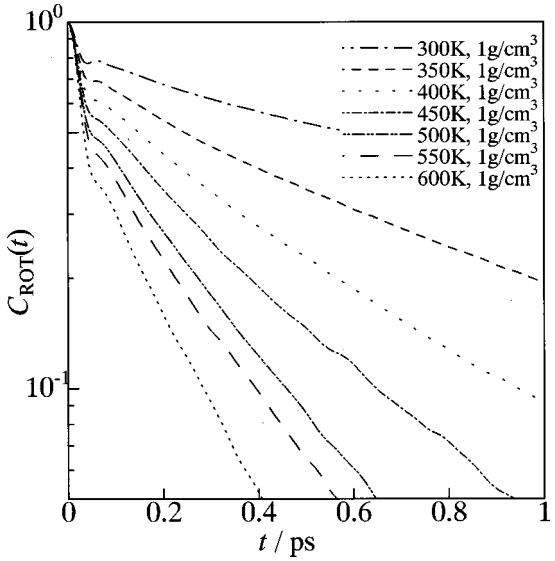

FIG. 11. Temperature dependence of rotational autocorrelation function along an isochore at 1 g/cm^3.

counterpart of the change in the fluid structure, i.e., from the icelike one to the simple-liquidlike one. A rate determining step of the diffusion of water molecules is an activation process to jump over potential barriers. The diffusion coefficient, thus, must be much influenced by the structural change of the fluid.[39] The diffusion coefficient was evaluated from the mean square displacement of water molecules. In Fig. 10, the calculated diffusion coefficient is presented as a function of inverse temperature, i.e., Arrhenius plot. The slope of the plot gives activation energy for the diffusion process. The plot can be divided into two limiting regions with different slopes: room temperature region near 280 K and high temperature region near 600 K. The activation energies of these two regions were 13 and 6.8 kJ/mol, respectively. The former is almost twice as large as the latter. The change of the slope seems to be continuous, corresponding to the continuous structural change as shown in Fig. 4. The barrier of the diffusion of water molecules becomes small, reflecting the break of the tetrahedral icelike structure.

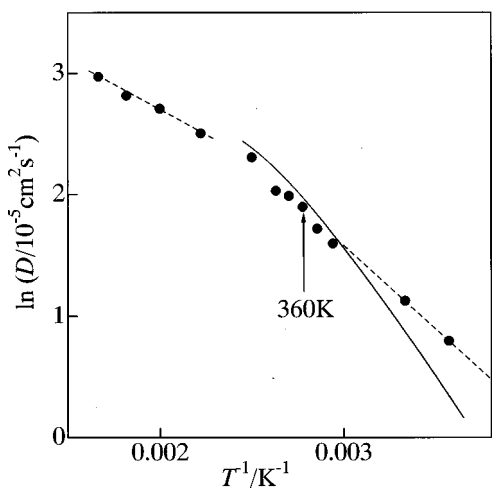

FIG. 10. Diffusion coefficient plotted against inverse temperature along an isochore at 1 g/cm^3. Closed circle: present calculation and solid line: experiment (Ref. 40).

D. Rotational dynamics

Rotational autocorrelation function is shown in Fig. 11 for the fluid at various temperatures of every 50 K. The function is defined by

$$C_{\mathrm{ROT}}(t) = \tfrac{1}{2}\langle 3\cos^2\theta(t) - 1\rangle, \tag{7}$$

where

$$\cos\theta(t) = \mathbf{y}(t)\cdot\mathbf{y}, \tag{8}$$

and $\mathbf{y}$ is the vector connecting the two hydrogen atoms in one molecule. The initial decay in the correlation function must be due to librational motion of the molecule in the cage formed by the surrounding molecules.[41] This is followed by the exponential decay of the rotational diffusion. As temperature increases, the relaxation becomes faster. Relaxation time was estimated by the numerical integration of the correlation function and plotted in Fig. 12. This must be related to the one observed by nuclear magnetic resonance experiment.[42] The correlation time decreased to be about 1/5 of the initial value when the temperature increased from 280 to 400 K. This may be ascribed to the structural change of the cage. Above 400 K, the correlation time decreases relatively slowly owing to weakening of the hydrogen bonds. Now, it is interesting to examine the dynamical behavior of polarization, which must be closely related to the rotational relaxation. Temperature dependence of relaxation times of the single molecular dipole moment and the polarization of the total system is plotted in Fig. 12, too. At 280 K, the relaxation times of the molecular dipole moment and the total polarization are 4.6 and 11.2 ps, respectively. At this temperature, the dynamical behavior of the total polarization must be dominated by the collective orientational relaxation in a three dimensional hydrogen-bonding network. The rela-

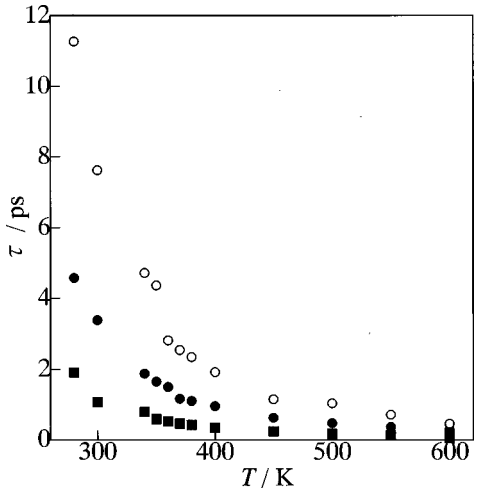

FIG. 12. Temperature dependence of rotational relaxation time of water molecule (closed square) and relaxation times of the single molecular dipole moment (closed circle) and the total polarization of the system (open circle) along an isochore at 1 g/cm^3.

tively rigid structure may give the large correlation time. With increasing temperature up to 400 K, the correlation time of the total polarization is substantially reduced and approaches the value for the single molecular polarization. It indicates that the relaxation process of the total polarization loses the collective character. This may be understood as a result of the collapse of the tetrahedral icelike structure. At higher temperatures, relaxation of the total polarization is mostly dominated by the single particle motions.

V. ISOTHERM AT 600 K

Properties of the supercritical water have been investigated at eight densities along an isotherm at 600 K. The density of the system ranges from the liquidlike one to the gaslike one, the latter being about one-tenth of the critical density ρ_c.

A. Spatial density correlation

The partial radial distribution functions g_{OO}, g_{OH}, and g_{HH} are presented in Fig. 13 for the fluid at six densities. All the functions at $\rho = 0.27$ g/cm^3 ($\approx \rho_c$) have a long-lived tail, which gives strong intensity of static structure factors in the small wave number region. This represents long-ranged strong density fluctuation found for the fluid near the critical point. However, in this study, we focus our discussion on the local fluid structure, since the number of water molecules, 256 in the present calculation, is too small to reproduce the correlation in the small wave number region, the so-called Ornstein-Zernike behavior.[43] In order to investigate this quantitatively, the calculation of a much larger system needs to be performed.[44]

For the oxygen-oxygen pair correlation function, the first peak shifts to larger separation with decreasing density. With respect to the height of the peak, as the density decreases and approaches ρ_c the first peak becomes lower. Contrary to this, at densities below $\rho = 0.27$ g/cm^3, the first peak grows up with decreasing density.[12] Then, the second peak around 6 Å

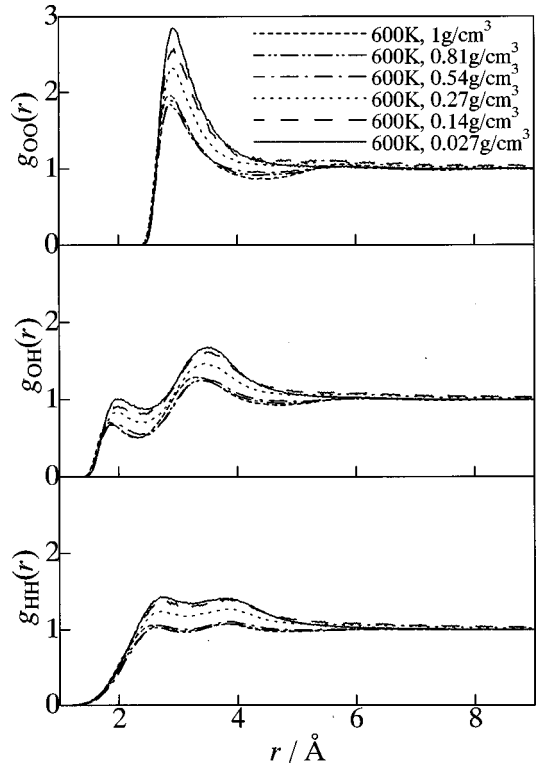

FIG. 13. Density dependence of oxygen-oxygen, oxygen-hydrogen, and hydrogen-hydrogen radial distribution functions, g_{OO}, g_{OH}, and g_{HH} along an isotherm at 600 K. The results are plotted for the fluid at six state points.

becomes weak and is not found for the fluid at 0.027 g/cm^3. In order to analyze the change of short-ranged fluid structure, the coordination number in the first coordination shell, $\langle n_{OO} \rangle$, and the ratio $\langle n_{OO} \rangle / \rho$ have been calculated and are presented in Fig. 14. The coordination number $\langle n_{OO} \rangle$ was evaluated by the numerical integration of g_{OO} up to 4.5 Å, which is the position of the first minimum in g_{OO} at 1 g/cm^3. As density decreases, $\langle n_{OO} \rangle$ decreases monotonically. On the other hand, at densities ranging from 1 to 0.405 g/cm^3,

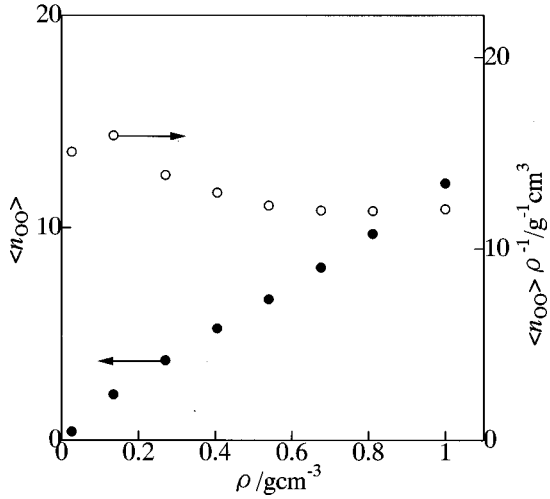

FIG. 14. Density dependence of average number of oxygen atoms in the first coordination shell with the radius of 4.5 Å, $\langle n_{OO} \rangle$, and the ratio, $\langle n_{OO} \rangle / \rho$, for the fluid at 600 K and 1 g/cm^3. Closed circle: $\langle n_{OO} \rangle$ and open circle: $\langle n_{OO} \rangle / \rho$.

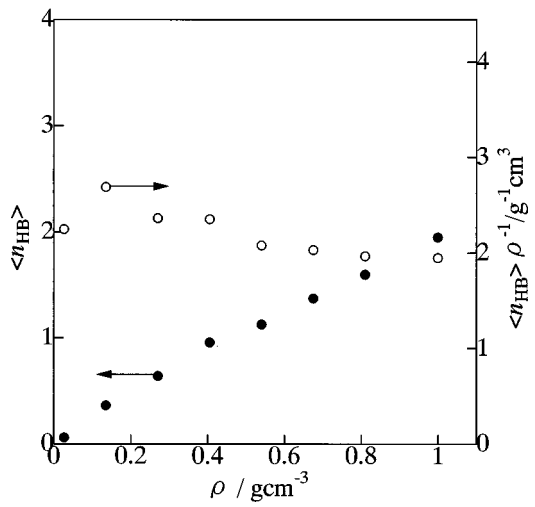

FIG. 15. Density dependence of average number of hydrogen bonds per molecule $\langle n_{HB} \rangle$ and the ratio, $\langle n_{HB} \rangle / \rho$, along an isotherm at 600 K. Closed circle: $\langle n_{HB} \rangle$ and open circle: $\langle n_{HB} \rangle / \rho$.

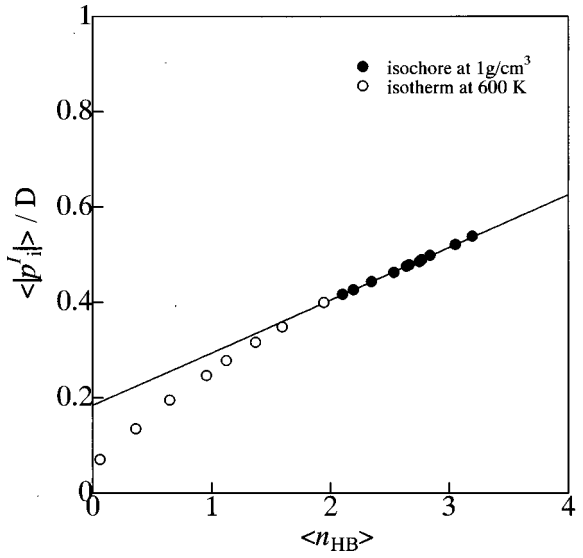

FIG. 16. Magnitude of induced dipole moment as a function of number of the hydrogen bonds.

$\langle n_{OO} \rangle / \rho$ is roughly constant. This indicates that the coordination number is almost proportional to the bulk number density. In more detail, however, the ratio $\langle n_{OO} \rangle / \rho$ deviates from the constant at densities below 0.27 g/cm^3. In this relatively low density region, decrease of the coordination number is slower than that of the bulk density. This may be caused by the preferential aggregation of molecules in the fluid. The behavior is also found in LJ fluid in the supercritical state.[45]

Oxygen-hydrogen pair correlation function, g_{OH}, has the first peak around 1.8 Å even at the lowest density we investigated. This indicates that the hydrogen bond between molecules may well be found even at the gaslike density. As stated above, the small deviation of the orientational distribution function from the constant value, shown in Fig. 8, represents the persisting hydrogen bonds, too. The less structured g_{HH}, however, implies that the orientational correlation among the molecules has almost diminished.

B. Hydrogen bond

Averaged number of hydrogen bonds $\langle n_{HB} \rangle$ is plotted in Fig. 15 as a function of density. As density decreases, $\langle n_{HB} \rangle$ decreases monotonically. The density dependence is similar to that of $\langle n_{OO} \rangle$. As is found in Fig. 8, the orientational correlation depends little on density. Thus, the density dependence of $\langle n_{HB} \rangle$ is dominated by the number of molecules in the first coordination shell, and the orientational correlation, which is related to the energy criterion of the hydrogen bond, gives minor contribution. The ratio of $\langle n_{HB} \rangle$ to the number density ρ is shown in Fig. 15, too. At densities higher than 0.54 g/cm^3, the ratio is approximately constant. However, the deviation from the constant value is noticeable at densities lower than 0.41 g/cm^3. This behavior is in agreement with that observed previously by the molecular dynamics calculation with the TIP4P model[11] as well as the nuclear magnetic resonance experiment.[26] It is worthwhile to note here that, in the density range we investigated, $\langle n_{HB} \rangle$ varies from 1.9 to 0.06. As discussed in Sec. IV B, a rule of thumb tells us that the percolation threshold is about 1.5 for any lattice system. It suggests that the percolated hydrogen bonds are broken into hydrogen-bonded clusters with decreasing density. The detailed analysis of the hydrogen-bonded clusters will be presented elsewhere.

Here, we examine the relationship between the magnitude of the induced dipole moment $\langle |p_i^I| \rangle$ and the average number of the hydrogen bonds $\langle n_{HB} \rangle$. In Fig. 16, $\langle |p_i^I| \rangle$ is plotted as a function of $\langle n_{HB} \rangle$. As $\langle n_{HB} \rangle$ decreases, the induced dipole moment becomes weaker. In the range $\langle n_{HB} \rangle = 1.9 \sim 3.2$, the magnitude of the induced dipole moment is linearly dependent on $\langle n_{HB} \rangle$. At $\langle n_{HB} \rangle$ smaller than 1.9, it deviates from the linear line. Now, it is interesting to extrapolate the linear line to $\langle n_{HB} \rangle = 4$, which is the number of hydrogen bonds in ice. The extrapolated $\langle |p_i^I| \rangle$ is 0.63 D. Since the magnitude of the permanent dipole moment of the RPOL mode is 2.02 D, the total dipole moment is calculated to be 2.65 D. This is in good agreement with the experimental value of the dipole moment of the water molecule in ice, 2.6 D.[28] Here, we assumed that the induced dipole moment is parallel to the permanent dipole moment.

C. Translational dynamics

Density dependence of velocity autocorrelation functions is given in Fig. 17. Oscillatory behavior found for the ambient water is not observed for the fluid at all the densities at 600 K. From the figure, two relaxation processes are found in the velocity autocorrelation function. One is the initial fast decay within $t = 0.1$ ps and the other is the slow relaxation over subpicosecond range. As density decreases, the relaxation becomes slower gradually. Long mean free path of the molecules in the low density fluid gives long-lived velocity correlation.

In Fig. 18, density dependence of the diffusion coefficients is presented together with the experimental result.[46] The RPOL model reproduces well the density dependence of the diffusion constant found in the experiment. As shown in

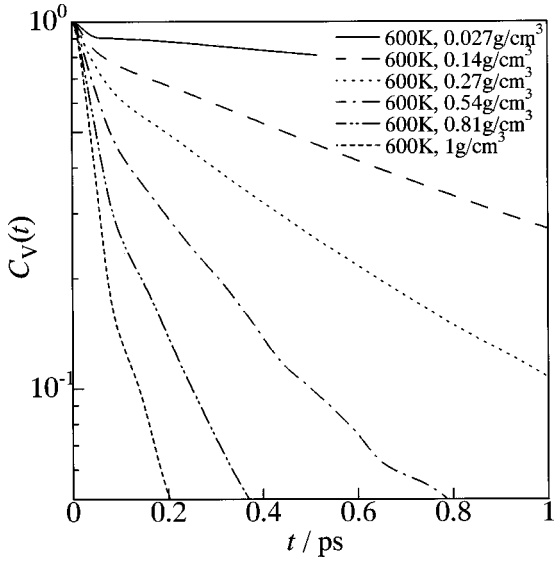

FIG. 17. Density dependence of velocity autocorrelation function along an isotherm at 600 K.

the inset of the figure, the diffusion coefficient is proportional to the inverse of the density at densities below the critical density. This indicates that the diffusion process in the low density region may be qualitatively described by the simple kinetic theory for gases. At densities above 0.68 g/cm^3, the deviation from the kinetic theory is noticeable. This may be caused by an increase of the coordination number in the first coordination shell.

D. Rotational dynamics

Density dependence of the rotational time correlation function is shown in Fig. 19(a). The functional form of the correlation functions changes gradually with decreasing density. Except for the fluid at the density lower than ρ_c, the correlation function consists of two components. Fast initial decay at $t<0.1$ ps must come from inertial rotation of the molecule. Exponential decay at larger t must be due to the rotational diffusion or reorientation of the molecule. Now, it is interesting to find that, at low densities, the functional form of C_{ROT} is much different from that found at higher densities. In particular, at the lowest density it is very similar to that of free rotor. This implies that, in the supercritical states, the rotational dynamics changes continuously from the liquidlike one to the gaslike one with decreasing density. The rotational relaxation time is presented in Fig. 19(b), too, which was estimated by numerical integration of the relevant correlation function. The correlation time has a minimum value as a function of density near the critical density. This is found for CF_3H fluid, too.[41] The behavior may be measured by nuclear magnetic resonance experiment.

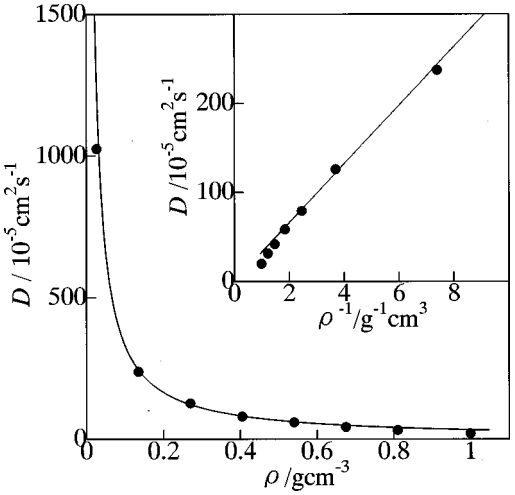

FIG. 18. Density dependence of diffusion coefficient along an isotherm at 600 K. Closed circle: present calculation and solid line: experiment (Ref. 46).

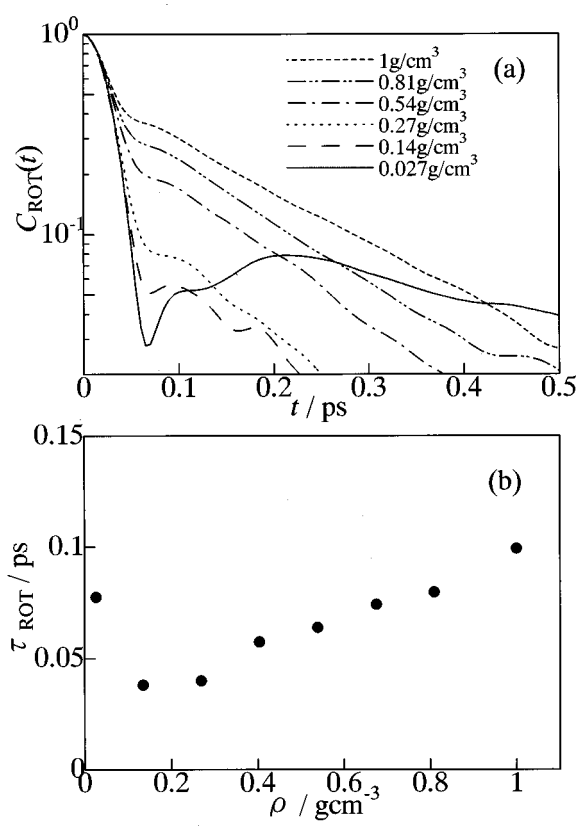

FIG. 19. Density dependence of (a) rotational autocorrelation function and (b) correlation time of the rotational relaxation along an isotherm at 600 K.

VI. CONCLUSION

A series of molecular dynamics calculations have been performed for water along an isochore at 1 g/cm^3 and an isotherm at 600 K. The results obtained from the present calculations may be summarized as follows. Along the isochore, the fluid structure changes from the tetrahedral icelike structure at room temperature to the simple-liquidlike structure at high temperatures. The structural change occurs continuously. At high temperatures, although icelike three body correlation of water molecules vanishes, there persist the hydrogen bonds between the molecules. The structural change gives marked effects to both the translational and rotational dynamics of water molecules. We found that the activation barrier of the diffusion at high temperature is about half as large as that at room temperature. Relaxation time of the

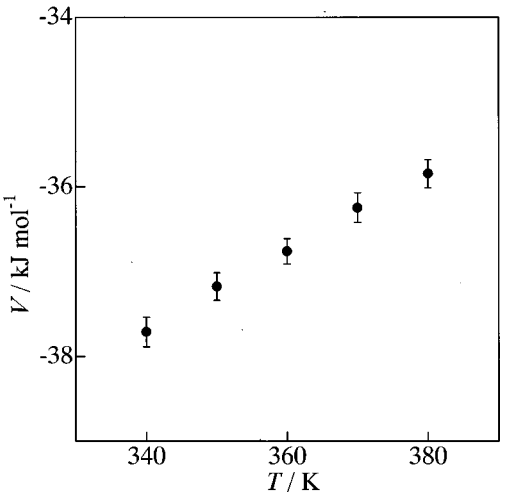

FIG. 20. Temperature dependence of the averaged potential energy along an isochore at 1 g/cm^3.

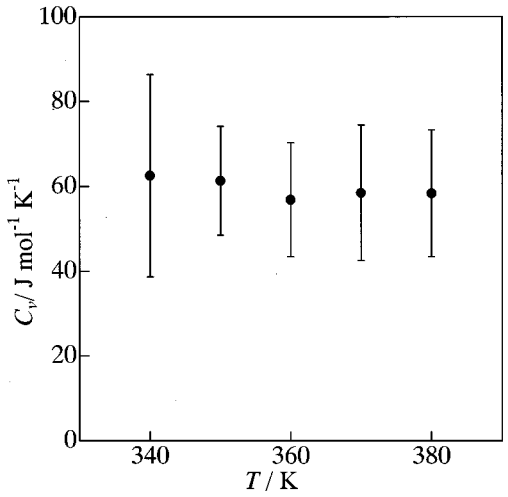

FIG. 21. Temperature dependence of the averaged constant volume specific heat along an isochore at 1 g/cm^3.

collective polarization fluctuation becomes substantially short with increasing temperature from 300 to 400 K. At higher temperatures than 400 K, the relaxation is dominated mainly by the single particle dynamics.

Along the isotherm, on the other hand, we observed long-lived tail in all the partial radial distribution functions near the critical density. The Ornstein-Zernike behavior in the small wave number region, however, could not be reproduced quantitatively due to the small system of the present study. As density decreases, the average number of hydrogen bonds per molecule changes from 1.9 to 0.06. This suggests that the percolated hydrogen bond in the system at high densities is broken into the clusters with decreasing density. At low densities, the translational dynamics is qualitatively described by simple kinetic theory for gases. At high density region, the diffusion coefficients deviate from the prediction by the kinetic theory. With respect to the rotational dynamics, the relaxation mechanism changes from the liquidlike one to the gaslike one continuously with decreasing density.

In order to reproduce quantitatively the long-ranged correlation representing the density fluctuation near the critical point, we need to perform the molecular dynamics calculations for a much larger system. From our experience of the large-scale molecular dynamics calculations of LJ fluid, we need the system containing more than 10 000 molecules in order to describe the Ornstein-Zernike behavior in the long wavelength region. Based upon 10 000 particle calculations, we could estimate the correlation length of the density fluctuation from the long wavelength correlation for the LJ fluid.[44] More important, however, is that we must clarify the molecular origin of long-ranged density fluctuation in the supercritical water. As suggested by this study, the system near the critical point consists of the hydrogen-bonded clusters. Larger-scale and long-time calculations will present a molecular picture of the clusters near the critical point.

ACKNOWLEDGMENTS

The authors thank the computer centers of the Institute for Molecular Science, Tokyo Institute of Technology, and Japan Atomic Energy Research Institute for the use of supercomputers. The work was supported in part by the Grant-in-Aid for Scientific Research (Nos. 09740419, 09440197, and 09216204) from the Ministry of Education, Science and Culture, Japan. N.Y. has been supported by the Japan Society for the Promotion of Science for Japanese Junior Scientists.

APPENDIX

In Sec. IV A, we showed that water changes its structure from the icelike one to the simple-liquidlike one with increasing temperature along the isochore. In this Appendix, we discuss whether the structural change indicates the presence of two liquid phases or not. In order to clarify the presence of phase transition along the isochore, we calculated thermodynamic quantities such as potential energy and constant volume specific heat C_v. Temperature dependence of the potential energy would show a hysteresis during the cycle of heating up and cooling down of the system if there exists first-order phase transition along the isochore.[47] If there is second-order phase transition, temperature dependence of C_v would show divergent behavior at the transition point.[43,48] First, in order to check the possibility of the first-order phase transition, we performed a set of MD calculations along the isochore. The MD runs were executed at temperatures ranging from 340 to 380 K with an increment of 10 K. We started from the low temperature side, i.e., 340 K, the final configuration of which was used as an initial condition for the next run at the higher temperature. We repeated the procedure at temperatures up to 380 K. When the temperature of the system reaches 380 K, the system was cooled down, in turn, from 380 to 340 K. The calculated potential energies along the isochore are presented in Fig. 20. The two values of the potential energy in the heating and cooling processes coincide with each other within 0.18 kJ/mol, and did not show any hysteresis. This indicates that the structural change is not of the first-order phase transition. Second, in order to examine the possibility of the second-order phase transition, we estimated C_v along the isochore from the fluctuation of the potential energy. Since, in gen-

eral, thermodynamic derivatives defined by fluctuation converge very slowly, we extended the MD calculation up to 200 ps at each temperature. The calculated C_v is presented in Fig. 21. It is noted that, since the RPOL model does not have intramolecular degrees of freedom, contribution from the vibrations is not included in the present C_v. In any case, divergent behavior is not found for C_v investigated. The C_v decreases monotonically with increasing temperatures. This indicates that there exists no second-order phase transition along the isochore. From the about discussion, we may conclude that the structural change does not come from any first- or second-order phase transition.

[1] E. Kiran and J. M. H. L. Sengers, *Supercritical Fluid: Fundamentals for Application* (Kluwer, Dordrecht, 1994).
[2] T. J. Bruno and J. F. Ely, *Supercritical Fluid Technology: Reviews in Modern Theory and Applications* (Chemical Rubber, Boca Raton, FL, 1991).
[3] E. V. Bright and M. E. P. McNally, ACS Symp. Ser. **488** (American Chemical Society, Washington, DC, 1992).
[4] E. Kiran and J. F. Brennecke, ACS Symp. Ser. **514** (American Chemical Society, Washington, DC, 1993).
[5] M. D. Luque de Castro, M. Valcárcel, and M. T. Tena, *Analytical Supercritical Fluid Extraction* (Springer-Verlag, Berlin, 1994).
[6] J. V. Sengers and J. M. H. L. Sengers, Annu. Rev. Phys. Chem. **37**, 189 (1986).
[7] C. A. Eckert, B. L. Knutson, and P. G. Debenedetti, Nature (London) **383**, 313 (1996).
[8] C. A. Eckert, D. H. Ziger, K. P. Johnston, and S. J. Kim, J. Phys. Chem. **90**, 2738 (1986).
[9] W. L. Jorgensen, J. Chandrasekhar, J. D. Madura, R. W. Impey, and M. L. Klein, J. Chem. Phys. **79**, 926 (1983).
[10] H. C. J. Berendsen, J. R. Grigera, and T. P. Straatsma, J. Phys. Chem. **91**, 6269 (1987).
[11] R. D. Mountain, J. Chem. Phys. **90**, 1866 (1988).
[12] R. D. Mountain, NIST Technical Report 6028 (1997); R. D. Mountain, Rev. High Pressure Sci. Technol. **7**, 1106 (1998).
[13] G. Löffler, H. Schreiber, and O. Steinhauser, Ber. Bunsenges. Phys. Chem. **98**, 1575 (1994).
[14] A. G. Kalinichev and J. D. Bass, Chem. Phys. Lett. **231**, 301 (1004).
[15] Y. Guissani and B. Guillot, J. Chem. Phys. **98**, 8221 (1993).
[16] P. T. Cummings, H. D. Cochran, J. M. Simonson, R. E. Mesmer, and S. Karaborni, J. Chem. Phys. **94**, 5606 (1991).
[17] E. S. Fois, M. Sprik, and M. Parrinello, Chem. Phys. Lett. **223**, 411 (1994).
[18] T. I. Mizan, P. E. Savage, and R. M. Ziff, J. Phys. Chem. **100**, 403 (1996).
[19] R. D. Mountain, J. Chem. Phys. **103**, 3084 (1995).
[20] A. A. Chialvo and P. T. Cummings, J. Chem. Phys. **101**, 4466 (1994).
[21] A. A. Chialvo and P. T. Cummings, J. Phys. Chem. **100**, 1309 (1996).
[22] M.-C. Bellissent-Funel, T. Tassaing, H. Zhao, D. Beysens, B. Guillot, and Y. Guissani, J. Chem. Phys. **107**, 2942 (1997).
[23] P. Postrino, R. H. Tromp, M. A. Ricci, A. K. Soper, and G. W. Neilson, Nature (London) **366**, 668 (1993); R. H. Tromp, P. Postrino, G. W. Neilson, M. A. Ricci, and A. K. Soper, J. Chem. Phys. **101**, 6210 (1994).
[24] A. K. Soper, F. Bruni, and M. A. Ricci, J. Chem. Phys. **106**, 247 (1997).
[25] K. Yamanaka, T. Yamaguchi, and H. Wakita, J. Chem. Phys. **101**, 9830 (1994).
[26] N. Matubayasi, C. Wakai, and M. Nakahara, Phys. Rev. Lett. **78**, 2573 (1997); J. Chem. Phys. **107**, 9133 (1997).
[27] A. C. Shepard, Y. Beers, G. P. Klein, and L. S. Rothman, J. Chem. Phys. **59**, 2254 (1973).
[28] C. A. Coulson and D. Eisenberg, Proc. R. Soc. London, Ser. A **291**, 445 (1966).
[29] L. X. Dang, J. Chem. Phys. **97**, 2659 (1992).
[30] N. Yoshii, H. Yoshie, S. Miura, and S. Okazaki, Rev. High Pressure Sci. Technol. **7**, 1115 (1998).
[31] S. Nosé, J. Chem. Phys. **81**, 511 (1984).
[32] M. P. Allen and D. J. Tildesley, *Computer Simulation of Liquids* (Clarendon, Oxford, 1987).
[33] D. Chandler, *Introduction to Modern Statistical Mechanics* (Oxford, New York, 1987).
[34] F. H. Stillinger and A. Rahman, J. Chem. Phys. **61**, 4973 (1974); R. W. Impey, M. L. Klein, and I. R. McDonald, *ibid.* **74**, 647 (1981); A. G. Kalinichev, Int. J. Thermophys. **7**, 887 (1986).
[35] G. Corongiu and E. Clementi, J. Chem. Phys. **97**, 2030 (1992).
[36] R. Ishii, S. Okazaki, I. Okada, M. Furusaka, N. Watanabe, M. Misawa, and T. Fukunaga, J. Chem. Phys. **105**, 7011 (1996).
[37] N. W. Dalton, C. Domb, and M. F. Sykes, Proc. Phys. Soc. **83**, 496 (1964); C. Domb and N. W. Dalton, *ibid.* **89**, 856 (1966).
[38] A. Geiger, F. H. Stillinger, and A. Rahman, J. Chem. Phys. **70**, 4185 (1979).
[39] M. Sprik, J. Chem. Phys. **95**, 6762 (1991); J. Phys. Chem. **95**, 2283 (1991).
[40] K. Krynicki, C. D. Green, and D. W. Sawyer, Faraday Discuss. Chem. Soc. **66**, 199 (1979).
[41] S. Okazaki, M. Matsumoto, I. Okada, K. Maeda, and Y. Kataoka, J. Chem. Phys. **103**, 8594 (1995).
[42] R. W. Impey, P. A. Madden, and I. R. McDonald, Mol. Phys. **46**, 513 (1982).
[43] H. E. Stanley, *Introduction to Phase Transition and Critical Phenomena* (Clarendon, Oxford, 1971).
[44] N. Yoshii and S. Okazaki, J. Chem. Phys. **107**, 2020 (1997).
[45] N. Yoshii, S. Miura, and S. Okazaki (unpublished data).
[46] W. J. Lamb, G. A. Hoffman, and J. Jonas, J. Chem. Phys. **74**, 6875 (1981).
[47] P. H. Poole, U. Essmann, F. Sciortino, and H. E. Stanley, Phys. Rev. E **48**, 4605 (1993).
[48] W. Gebhardt and U. Krey, *Phase Transition and Critical Phenomena* (Frider, Vieweg & Sohn, Braunschweig, 1980).